Heavy-ion Irradiations of Fe and Fe-Cr Model Alloys Part 2: Damage evolution in thin-foils at higher doses

Mercedes Hernández-Mayoral, Zhongwen Yao, Mike Jenkins, Mark Kirk

Heavy-ion Irradiations of Fe and Fe-Cr Model Alloys Part 2: Damage evolution in thin-foils at higher doses

Journal:	*Philosophical Magazine & Philosophical Magazine Letters*
Manuscript ID:	TPHM-08-Feb-0047.R1
Journal Selection:	Philosophical Magazine
Date Submitted by the Author:	15-Jul-2008
Complete List of Authors:	Hernández-Mayoral, Mercedes; CIEMAT, Division of Materials Yao, Zhongwen; University of Oxford, Materials Jenkins, Mike; University of Oxford, Materials Kirk, Mark; Argonne National Laboratory, Materials Science
Keywords:	in-situ electron microscopy, radiation damage
Keywords (user supplied):	FeCr alloys

Note: The following files were submitted by the author for peer review, but cannot be converted to PDF. You must view these files (e.g. movies) online.

video 1 paper 2.mpg
video 2 paper 2.mpg
video 3 paper 2.mpg
video 4 paper 2.mpg
video 5 paper 2.mpg
video 6 paper 2.mpg
video 7 paper 2.mpg

Heavy-ion Irradiations of Fe and Fe-Cr Model Alloys

Part 2: Damage evolution in thin-foils at higher doses

M. Hernández-Mayoral[*], Z. Yao[**], M. L. Jenkins[**1] and M. A. Kirk[***]

[*]Division of Materials. CIEMAT Avenida Complutense, 22, 28040-Madrid
[**]Department of Materials, University of Oxford, Parks Rd., OX1 3PH
[***]Materials Science Division, Argonne National Laboratory, Argonne, IL 60439

[1] Corresponding author: Email mike.jenkins@materials.ox.ac.uk

Abstract

We continue our study of heavy-ion damage in Fe and FeCr alloys started in Part 1[1] with an investigation of damage development in UHP Fe and Fe8%Cr at higher doses up to 2 x 10^{19} ions m^{-2} (~13 dpa). In thin-foil irradiations with 150 keV Fe^{+} ions at 300°C and room temperature (RT), more complex microstructures started to develop in thicker regions of the foils at doses greater than about 2 x 10^{18} ions m^{-2}, seeming to involve cooperative interaction, alignment and coalescence of smaller loops. First strings of loops all with the same ½<111> Burgers vectors formed. In UHP Fe irradiated at 300°C the damage then developed into colonies of resolvable interstitial loops with ½<111> Burgers vectors. By a dose of 2 x 10^{19} ions m^{-2}, large (several hundred nanometre) finger-shaped loops with large shear components had developed by the growth and subsequent coalescence of smaller loops. Similar but finer-scale damage structures developed in UHP Fe irradiated at RT and in Fe8%Cr irradiated at both RT and 300°C.

Deleted: not identical

Keywords: heavy-ion irradiation, FeCr alloys, *in-situ* TEM

§1 Introduction

In Yao *et al* [1], hereafter called Part 1, we described the evolution of radiation damage under heavy-ion irradiation at room temperature (RT) and 300°C in thin foils of pure Fe of different purities and a range of FeCr alloys at doses up to 2 x 10^{18} ions m^{-2}. In this paper we continue with a description of the damage structures which evolved at higher doses up to 2 x 10^{19} ions m^{-2} in ultra high-purity Fe (UHP Fe) and Fe8wt.%Cr under 150 keV Fe^+ irradiation at 300°C and at RT.

§2 Experimental details

The UHP Fe and the Fe8wt.%Cr alloys were the same materials described in Part 1. Both were polycrystalline materials with the majority of grains oriented within 0-15° of (111). The experimental methods were also largely the same. Specimens were investigated in both *ex-situ* TEM and *in-situ* experiments. In *ex-situ* experiments, specimens of UHP Fe were irradiated with 150 keV Fe^+ ions at 300°C in the CSNSM Facility in Orsay, France to doses from 10^{18} to 2 x10^{19} ions m^{-2} at a dose rate of 4 x 10^{15} ions m^{-2} s^{-1}. They were returned to CIEMAT in Madrid for examination in a JEOL 2010 transmission electron microscope. *In-situ* experiments were carried out on the Argonne IVEM-Tandem Facility, as described in Part 1. Specimens of UHP Fe and Fe8%Cr were irradiated with 150 keV Fe^+ ions at 300°C or RT to maximum doses of about 2 x 10^{19} ions m^{-2}. The depth of the peak damage for 150 keV Fe^+ irradiation is at about 28 nm and damage extends to a maximum depth of about 100 nm. A dose 2 x 10^{19} m^{-2} of 150 keV Fe^+ ions gives a maximum damage level of ~ 13 dpa. The maximum dose in the *in-situ* experiments was limited by the accelerator ion source lifetime, and it was not always possible to reach 2 x 10^{19} ions m^{-2}. The evolution of damage over the whole dose range was followed by recording images dynamically under weak-beam diffraction conditions. The irradiation was carried out in several dose steps, and after each step micrographs were recorded on film or CCD. After the maximum dose was achieved the specimens were allowed to cool to room temperature (if irradiated at 300°C) for further detailed microscopy.

Due to the development of larger, more complex damage structures, more complete diffraction contrast experiments were performed than at lower doses. For example, in the experiment in UHP Fe at 300°C described in §3.1 we succeeded in tilting a specimen oriented about midway between the [111] and [110] poles to both of these poles, as well as to the [311] and [131] poles. Both weak-beam and bright-field kinematical (BFK) micrographs were taken in all available reflections. The |**g.b**| table for this experiment is given in table 1, and shows that a complete analysis of Burgers vectors is possible. In most cases micrographs were taken with both +**g** and –**g**. It was then possible to deduce the vacancy or interstitial nature of resolvable loops from their inside-outside contrast behaviour (for details see [2]). In other cases it was not possible to carry out such an extensive analysis because of difficulties in tilting ferromagnetic specimens, but less extensive experiments still proved informative.

§3 Results

3.1 UHP Fe irradiated at 300°C

Figure 1 shows an overview of damage development in *ex-situ* experiments over a dose range of 2 x 10^{18} ions m^{-2} to 2 x 10^{19} ions m^{-2} (1.3 - 13 dpa). The micrographs were taken in a moderately thick (60-100 nm) area of foil. They should be compared with the micrographs presented in Part 1 (e.g.

Deleted: (~ 1dpa).

Deleted: In all these experiments the damage took the form of small (2-5 nm) dislocation loops with Burgers vectors **b** = ½<111> or <100>. Loops were seen only at cascade overlap doses. There was evidence that some at least of the loops were vacancy in nature. Loop number densities N increased with dose φ at a rate $N = \varphi^n$ with n ≈ 0.7 ~2 depending on material and irradiation conditions. The main effect of Cr seemed to be in reducing loop mobilities. Less loop "hopping" was seen in FeCr alloys than in pure Fe, and fewer loops were lost to the foil surfaces. The irradiation temperature also affected loop mobilities: more loop hopping was seen at 300ºC than at RT and this led to greater loss of loops at the higher temperature.

Deleted: in thin foils

Formatted: Indent: First line: 0.5"

Formatted: Font: Italic

Deleted: Again specimens were investigated by both *ex-situ* TEM and *in-situ* experiments using the

Deleted: Irradiations were carried out

Deleted:

Deleted:

Deleted: 12

Deleted: (see Part1).

Deleted: As described in Part 1 [1] a

Deleted: of

Deleted: ¶

Deleted: ¶

Deleted: We first present the results of *ex-situ* experiments.¶

Formatted: Indent: First line: 0"

Deleted: ¶

Formatted: Font: Italic

Deleted: Figure 1(a) and (b) show

Deleted: in

Deleted: over a dose range 2 x 10^{18} ions m^{-2} to 2 x 10^{19} ions m^{-2} (1.3-13 dpa). It

Deleted: These micrographs

Figure 1) where the spatial distributions of loops appeared random. By a dose of 2 x 10^{18} ions m^{-2} (Figure 1(a)), the loops are no longer randomly distributed. Strings of 4-~10 small loops have developed, still visible at this stage as dark dots rather than resolved loops and forming short chains with no obvious alignment direction. By a dose of 10^{19} ions m^{-2} (Figure 1(b)) chains of resolved loops are visible. In this region of an [001] foil the chains are aligned along or close to the [110] direction perpendicular to the diffraction vector $\mathbf{g} = 1\bar{1}0$. Figure 1(c) shows the further development of damage at a dose of 2 x 10^{19} ions m^{-2} in a wedge-shaped specimen. In areas of foil of thickness > 100nm at the left of the micrograph, a dense dislocation network has formed. Large elongated loops appear at intermediate foil thicknesses. Diffraction contrast experiments showed that these large loops have Burgers vectors **b** = ½<111> and inside-outside contrast analysis indicated they are of interstitial nature. All ½<111> loop variants were present in most foils, although in local areas a single variant (or occasionally two of the variants) often predominated. In very thin areas (< 50 nm) to the far right of the micrograph of Figure 1(c) only isolated loops are present, most of which have **b** = <100>. All variants were present. It was not possible to establish the nature of these loops.

Measurements of loop size distributions obtained from these and similar micrographs are shown in Figure 2. The size measured was the maximum dimension of the loop. There is a tendency for loop sizes to increase with dose, unlike the situation at lower doses (Part 1). Further quantitative data are shown in table 2 (together with data for Fe8%Cr, see §3.3 below). At the highest dose in UHP Fe there was a broad distribution of loop sizes with a tendency towards a bimodal distribution consisting of populations of small loops and larger elongated loops. In this case the average maximum sizes of the two distributions are given separately. Note that the loop number density in UHP Fe decreased at the highest dose. This is due to loop coalescence which is described explicitly below.

Further insight into this complex microstructure was obtained by *in-situ* experiments. Figure 3 shows how the microstructure developed with dose from 10^{18} – 1.6 x 10^{19} m^{-2} in one area of thickness about 100 nm, as determined by counting thickness fringes. The same field of view is shown in each micrograph. Video sequences[2] 1-4 show damage development at these different doses, and should be viewed in conjunction with Figure 3. In early stages of the irradiation, at doses ≤ 5x10^{17} ions m^{-2} (~0.3 dpa, see video 1) small dislocation loops were homogeneously distributed with no tendency to cluster. The loop mobility during irradiation was very high, with many loops executing discrete jumps parallel to their Burgers vectors sometimes of amplitude > 10 nm, as described in Part 1. At doses above about 10^{18} ions m^{-2} (0.6 dpa, Figure 3(a)) a gradual change took place. Neighbouring loops appeared to interact elastically to form first small loosely-attached groups and then strings of several loops. Initially the small groups or strings were unstable, often breaking up. New loops appeared in the vicinity of others. The process was difficult to follow in detail even in frame-by-frame analyses of videos, and so the exact mechanism by which the strings formed is still unclear. As the irradiation proceeded the strings became more stable (see Figure 3(b), and video 2). The strings did not yet coalesce, which may indicate that self-climb of small clusters is low at this temperature.

At doses above about 5 x 10^{18} ions m^{-2} (~3 dpa) resolvable dislocation loops (of size > 10 nm) developed, certainly at the positions of loop strings and apparently by their coalescence. Such well-resolved loops are seen in Figure 3(c) at a dose of 10^{19} m^{-2} (6.5 dpa). The process by which loop strings

[2] In order to play these .mpg files with RealPlayer you may need to install a mpeg-2 video codec, which is widely available as a free download on the web.

Deleted: shown

Formatted: Font color: Auto

Deleted: At higher doses large, often elongated loops were seen, (Figure 1(c)). Diffraction contrast experiments showed that the large loops had Burgers vectors **b** = ½<111> and inside-outside contrast analysis indicated they were of interstitial nature. The dependence of damage on the foil thickness is seen clearly in Figure 2 which shows a wedge-shaped specimen irradiated to a dose of 2 x 10^{19} ions m^{-2}. In areas of foil of thickness > 100nm a dense dislocation network formed at this dose (Figure 2(a)). Elongated loops appeared at intermediate foil thicknesses, with **b** = ½<111>. In very thin areas (< 50 nm) to the far right of the micrograph of Figure 2(b) only isolated loops were present, most of which had **b** = <100>.

Deleted: 3

Deleted: For the three lower doses, the second column shows the average maximum loop sizes.

Deleted: The third column gives the size of the largest loop seen at the different doses. The right-hand column shows areal number densities (loops m^{-2}). The use of areal densities, as in Part 1, is perhaps less justified at the higher doses of the present experiments when more complex microstructures develop.

Deleted: 4

Formatted: Superscript

Formatted: Superscript

Formatted: Superscript

Deleted: dynamically

Deleted: 4

Deleted: , Figure

Formatted: Font: Not Bold

Deleted: 4

Deleted: 3(a) and

Formatted: Font: Not Bold

Deleted: 4

Deleted:), which is similar to figure 1(b)

Deleted: (

Deleted: 4

Formatted: Superscript

Formatted: Superscript

Deleted:)

developed into resolvable loops was captured in video 3, which shows an UHP Fe specimen irradiated at 300°C over a dose range 6.5 to 6.6 x 10^{18} ions m^{-2}. Figure 4 shows a series of frames extracted from this video.

With further irradiation these loops grew, Figure 3(d). Video 4 shows that this growth process was not uniform. Figure 5 shows several video frames, although the video itself should be viewed to appreciate the whole process. Individual loops seemed to flex or "breathe", and gradually increased in size, although occasionally individual loops shrank significantly for a time before continuing to grow. Small white dots (in these weak-beam images) were frequently seen decorating larger resolved loops (see e.g. the arrowed features in the left-hand panel of Figure 5). The contrast of these decorating features always faded after some time, suggesting that the climb of larger loops involved the assimilation of smaller loops, perhaps by a change of Burgers vector (see subsequent panels of Figure 5)[3]. However, increases and decreases in loop size – flexing - occurred without the obvious involvement of smaller loops. Large loops often developed in lines, sometimes along or close to <110> directions.

When loops overlapped they sometimes coalesced to form larger finger-shaped loops, often several hundred nanometres in length and several tens of nanometres in width (Figure 5, and video 4). Generally loops lay entirely in the specimen, despite reaching these large sizes. Occasionally loops intersected the foil surface. Even more occasionally large loops were seen to glide out of the foil (see also section 3.3, and video 7). There was a tendency for finger-shaped loops to align close to <110> directions, as in Figure 1(b). However the particular direction in which they aligned in a given area tended to be such that the long-axis of the loops pointed towards the hole in the wedge-shaped foil, that is, in the direction of the thickness gradient (see Figure 1(c)).

Figure 6 shows some representative BFK micrographs selected from the full diffraction contrast experiment which was performed at the end of the irradiation (table 1). The foil normal was oriented about 15° away from the [111] pole in the direction of the [110] pole as shown schematically in the stereogram of Figure 7. This area contained three sets of large loops, members of which are labeled A, B and C. Set A had developed in this region into elongated finger-like loops such as those seen in Figures 1(c) and 5, although in this area they are not as dominant. Sets B and C comprise more isolated rounded loops. Smaller loops visible as dark dots are also present. There are also dark dots decorating the larger loops. Loop sets A and B are visible in Figure 6(a) and (d), which show a ±**g** pair with **g** = $\bar{1}10$ taken close to the [111] pole. The finger-loops marked A show outside contrast in Figure 6(a) with **g** = $\bar{1}10$ and inside contrast in figure 6(d) in **g** = $1\bar{1}0$. The second set of more rounded large loops B show the reverse contrast. Inside-outside contrast was also observed in two other reflections, not shown here. The set of loops A is out of contrast in Figure 6(b) with **g** = $01\bar{1}$ but is visible in all the other micrographs here. The full contrast experiment found that set A was also out of contrast in **g** = $1\bar{1}2$, and so confirms that the Burgers vector of these loops is **b** = ± ½[$\bar{1}11$]. Similarly the Burgers vector of loop set B which is out-of-contrast in **g** = $10\bar{1}$ (Figure 6(c)) and **g** = $\bar{1}12$ (not shown) is **b** = ± ½[$1\bar{1}1$]. The third set of rounded loops C is out-of-contrast in Figure 6(a) and (d) but can be seen in Figures 6(b, c and e) and so has **b** = ± ½[$11\bar{1}$]. These Burgers vectors are also shown on the

[3] Climb of pre-existing line dislocations also seemed to involve interaction with and assimilation of small loops, see e.g. video 2.

Deleted: well
Deleted: 5
Deleted: ¶
Deleted: 4
Deleted: 6
Deleted: 6
Deleted: 6
Deleted: 6
Deleted: ¶
Deleted: ¶
Figure 7 shows loop alignment more clearly. Here the same specimen seen in Figure 6 has been tilted to [001], and a nearby area showing more organized loop alignment has been imaged under BFK conditions. Lines of loops can be seen along or close to the [$\bar{1}10$] direction running diagonally from the top left, and some have coalesced to form finger-shaped loops, similar to those seen in figure 1(b). These loops belong to the set designated A in the Burgers vector analysis described below. The [$\bar{1}10$] direction along which they align lies close to the plane of the foil. The tendency for alignment shown in this micrograph may be exaggerated because the foil has been tilted such that the loop habit plane, which is close to the plane of the foil, is inclined, see below. There is some evidence for more limited alignment in the perpendicular [110], direction which is steeply inclined to the foil plane, suggesting the formation of a raft-like structure. ¶
¶
... [1]
Deleted:
Deleted: , see Figure 8
Deleted: 9
Deleted: 10
Deleted: ,
Deleted: 6
Deleted: 7
Deleted: 9
Deleted: 9
Deleted: 9
Deleted: 9
Deleted:
Deleted: 9
Deleted: 9
Deleted: 9
Formatted: English (U.K.)

stereogram. Attempts to determine the Burgers vectors of the smallest loops (visible only as small dots) were not successful.

Information on the habit planes of the loops was obtained from the changes in their projected shapes when the foil was tilted to the various poles [111], [110], [311] [131] and [001]. The set of elongated loops A narrowed somewhat but did not become edge-on when the foil was tilted to [110] showing these loops do not lie on $(\bar{1}11)$ and so are not of pure edge type. In fact they seem to lie close to or on the (111) plane which is shallowly inclined about 15° to the plane of the foil. Three other observations are consistent with these loops lying close to the foil plane. First, they grew to large sizes in both dimensions without intersecting the foil surface except in rare cases. Second, weak-beam images of the loops showed no strong depth oscillations, so the bounding dislocations cannot be steeply inclined. Third, the projected shapes of loops which are elongated along $[\bar{1}10]$ when viewed along a direction close to [001] is consistent with a habit plane close to (111). It was more difficult to determine the habit planes of the other sets of loops B and C, but most of these are also thought to have large shear components. The jagged shapes of some of the loops suggest however that they may not lie on a single plane, but are possibly stepped.

The nature of the loops was established from a knowledge of their Burgers vectors, habit planes and inside-outside contrast behaviour. For the orientations used for imaging the inside-outside contrast behaviour was expected to be the same as for an edge loop of the same Burgers vector (the loop normals $\mathbf{n}_L$ lie within the region of the stereogram centred on the beam-direction **z** and bounded by the great circles **n.b** = 0 and **n.z** = 0, see ref [2] p80 and Figure 7). In all cases the contrast changes of the large resolvable loops (sets A, B and C) were consistent with loops of interstitial nature.

Figure 8 shows evidence for the possible presence of small voids in a specimen irradiated at 300°C to a dose of 10^{19} ions m^{-2}. These images were taken in a thin area of foil with the specimen oriented such that little diffraction contrast was present. Very small (1-2 nm) circular features are present, which appear black in the over-focused image on the left and white in the under-focused image on the right. This is consistent with the contrast expected from small voids. Similar features were not present in unirradiated specimens, or in specimens irradiated to lower doses.

3.2 UHP Fe irradiated at RT

The initial stages of damage development were similar to the irradiation at 300°C. Again at low doses small loops were produced homogeneously. Again the video (5) showed that small loops in thicker areas (≥ 60 nm) were very mobile (although the frequency of hopping was less than at 300°C – see Part 1). At a dose of 10^{19} ions m^{-2} strings of loops had formed in thicker areas of foil (Figure 9). However these strings had not developed further when the irradiation was terminated at a dose of 1.6 x 10^{19} ions m^{-2} (~ 10 dpa). The specimen was then tilted to an [001] orientation. At this orientation the strings were visible as two more or less perpendicular sets, lying close to the 110 and $1\bar{1}0$ directions. A contrast experiment showed that each string consisted of loops with the same ½<111> Burgers vector.

3.3 Fe8%Cr irradiated at 300°C and RT

The evolution of the damage microstructures in Fe8%Cr is illustrated in Figure 10 (for the 300°C irradiation) and Figure 11 (for RT). In both cases the foil thickness was about 100 nm. The damage evolution was qualitatively similar to damage evolution in UHP Fe, and again was characterized first by the development of strings of loops at doses above about 10^{19} ions m^{-2} (see video

Deleted: and

Deleted: A stereo pair taken with **g** = $\bar{1}10$ is shown in Figure 11 (a) and (b). The members of this pair were taken a few degrees from the [111] pole and the [110] pole respectively and so are approximately equidistant from the foil-normal orientation about mid-way between these poles. Consistent with this, the separation of loops is nearly the same in the two micrographs. The sizes and shapes of individual loops change however.

Deleted: In Figure 11(a) the loops are viewed nearly flat-on and have a maximum width. In Figure 11(b) they have been tilted a further 30° about the $\bar{1}10$ **g**-vector and so are now inclined by about 35°. The consequent foreshortening has been simulated in Figure 11(c) by shrinking the image of Figure 10(a) in the x-direction perpendicular to **g** by a factor cos35° = 0.82. Note that the shapes and sizes of many of the loops in Figure 11 (b) and (c) now match fairly well.

Deleted:

Deleted: as in Figure 7

Deleted: is

Deleted: 10

Deleted: 12

Deleted: s

Deleted: s

Deleted: ¶

Deleted: ¶

Deleted: This will be analysed in greater detail in a later paper

Deleted: 13

Deleted: js

Deleted: and the contrast experiment illustrated in Figure 14 was performed. In Figure 14(a), taken in **g** = 002,

Deleted: of strings are seen

Deleted: When imaged in **g** = 110 or **g** = $1\bar{1}0$ (Figure 14(b) and (c)) only the set of strings perpendicular to **g** is seen. This is consistent with e

Deleted: i

Deleted: ng

Deleted: ¶

Deleted: 15

Deleted: 16

6 and Figures 10(a) and 11(a)) which further developed into resolvable dislocation loops at a dose of about 2 x 10^{19} ions m^{-2} (Figures10(b) and 11(b)). Video 7 shows the loss of a large loop by glide from the foil, which was seen only rarely. At 300°C there was evidence that oriented arrays of finger-like loops were starting to form (Figure 10(b)), although this was on a finer scale and not as obvious as in UHP Fe. Quantitative data on loop sizes and number densities for this condition are shown in table 2. At the highest dose loops as large as 24 nm were present, but extensive loop coalescence had not taken place and loop number densities continued to increase, unlike the case of UHP Fe. In the RT irradiation at this dose, loop strings, some of which had developed into a network of large resolvable loops, were present (Figure 11(b)).

Deleted: .
Deleted: of a large loop
Deleted: 15
Deleted: c
Deleted: 16
Deleted: d

4. Discussion

Deleted: ¶
Formatted: Numbered + Level: 1 + Numbering Style: 1, 2, 3, … + Start at: 4 + Alignment: Left + Aligned at: 0.25" + Tab after: 0.75" + Indent at: 0.75"

We are now in a position to speculate on the underlying radiation damage mechanisms leading to our observations. A first point to make is that our observations are limited by the resolution limit in diffraction contrast imaging. We see only clusters of size larger than about 1-2 nm (the lower limit depending on foil quality) and such clusters comprise of the order of 100 point defects. Smaller clusters are certainly present, probably in higher concentrations, but we are not able to observe these directly.

The initial production of dislocation loops.

Deleted: ¶

In our experiments most point defects are created in high-energy cascades initiated by incoming ions. It has long been accepted that a likely result of the cascade process is the production of a vacancy-rich core surrounded by a shell of interstitials. In many materials the vacancy-rich cores may collapse to form dislocation loops visible in the TEM. This does not seem to happen in Fe in cascades initiated by Fe^{+} ions or Fe primary knock-on atoms [3,4]. Instead the vacancies may aggregate to form micro-voids or loose vacancy sponges, not visible in the TEM but detectable by positron annihilation experiments, see e.g. [5]. It is now thought, on the basis of several molecular dynamics (MD) studies e.g.[6-8] that interstitial clustering also occurs spontaneously in cascades without the need for long-range diffusion. Experimental evidence for interstitial clustering in cascades in Fe is lacking, although small (~ 3 interstitial) clusters have been found in X-ray diffuse scattering experiments on neutron-irradiated Al at temperatures below Stage I [9]. The interstitial clusters seen in MD simulations of cascades in Fe typically consist of a few to tens of interstitial atoms, again too small to be seen directly in the TEM. The stable configuration of these small clusters can be regarded as a set of <111> crowdions. They are highly mobile in one dimension.

Deleted: the

Our experiments are certainly not inconsistent with this picture. We see no defects of any kind at low doses where cascades are well separated spatially. This implies that clusters of visible size are not produced in individual cascades. Damage first appears at cascade overlap doses and takes the form of small 2-5 nm dislocation loops. We have presented evidence in Part 1 that at least some of these loops are created in a cascade process.

Deleted: This evidence includes: (1) the areal density of loops does not depend on the foil thickness (Part 1, Fig.4); and (2) the loops do not increase in size at doses below about 10^{18} ions m^{-2}, that is before loop interactions and the development of a more complex microstucture (Part 1, Figures 7 and 8). Of course both of these measurements were made from micrographs taken after irradiation, and so exclude loops lost during irradiation.

What is this cascade process? The production of vacancy loops by the collapse of individual cascades has been seen in experiments on pure Fe irradiated with Xe^{+} and other very heavy ions [10]. Cascade collapse is therefore possible in Fe, but probably only in cascades which result in higher vacancy concentrations and energy densities than those produced by self-ions. It has been argued that the collapse of cascades initiated by self-ions can occur if the cascade occurs in a region populated with sub-microscopic clusters remaining from earlier cascades, so-called cascade debris, see Part 1 and refs [3,4]. Our observations are again not inconsistent with this picture. The observation of small resolvable

Formatted: Font color: Blue
Deleted: We note that the

voids at high doses suggests the presence of unresolved vacancy clusters at lower doses. In addition the time-dependence of loop formation reported in Part 1 suggests that loops grow by the diffusion of point-defects or small clusters from their immediate surroundings over a period of one or two tenths of a second. This is consistent with an initial collapse event leading to the production of a small loop. The loop then grows by accretion of nearby vacancies within the cascade volume.

This loop formation process was envisaged for the production of vacancy loops at overlap doses. Could a similar process result in the production of visible *interstitial* loops? There seems no reason to exclude this *a priori*, although it may seem less likely than vacancy loop formation, since cascade debris is likely to consist of small *immobile* vacancy clusters such as microvoids, but very *mobile* interstitial clusters which may leave the scene before the arrival of a subsequent cascade. Perhaps it is more likely that interstitial loops are formed by random encounters between migrating sub-microscopic interstitial clusters. The increase in cluster sizes at doses above 10^{18} ions m^{-2} (table 2) suggests that some clusters grow in this dose regime by diffusion and coalescence processes.

In our *in-situ* experiments we were not able to determine the nature of the mobile loops directly. In Part 1, we showed that some of the loops in Fe11%Cr produced by 30 keV Ga^+ ion irradiation at overlap doses in a FIB are most likely vacancy in nature. However we also noted that the loops which we had analysed lay close to the foil surface (in the first depth layer) in foils of moderate thickness (≤ 50 nm). They were also fairly large in size and immobile. They may therefore not be typical of the whole population of loops seen in our experiments. It is likely that many if not most loops in this (111) foil would have been lost to the surface. This might include particularly interstitial loops with **b** = ½ <111> which are likely to be highly mobile. We conclude that vacancy loops are very likely to be present in our experiments, but we cannot exclude the possibility that interstitial loops are also formed, perhaps in comparable or even higher numbers. Abe *et al* [11] have argued that many of the small mobile clusters generated from individual displacement cascades in copper and gold by *in-situ* heavy-ion irradiation are of interstitial character. The interstitial nature of the clusters in these experiments was not determined directly but was inferred from their short lifetimes (a few thirtieths of a second – sessile vacancy clusters such as Frank loops or stacking-fault tetrahedra had much longer lifetimes).

The development of loop strings

In thin regions of foil (≤ 40 nm) only isolated loops were seen at all doses, most with <100> Burgers vectors. From the discussion above we speculate that these are relatively immobile vacancy loops, produced by a cascade overlap mechanism. At these foil thicknesses both of the surfaces act as strong sinks for the mobile interstitial clusters and large interstitial loops are unlikely to form. Probably some vacancy loops will also be lost to the surface. However, at doses above about 2 x 10^{18} ions m^{-2} strings of loops appeared in thicker regions of foil. Loop strings consist typically of several small loops, all with the same ½ <111> Burgers vector, and aligned roughly along <110> directions. The formation of these strings appeared to involve some sort of cooperative interaction between mobile loops.

The formation of loop strings seems similar to the early stages of raft formation, which is seen in many materials but is particularly prevalent in bcc metals, see e.g. [12-14]. Raft formation in irradiated materials has been discussed recently by Wen *et al* [15]. These authors found in Kinetic Monte Carlo simulations that raft formation can be achieved by the prismatic glide of one-dimensional (1-D) interstitial clusters and rotation of their Burgers vectors under the influence of internal strain

Deleted: point-defects
Formatted: Font: Italic
Deleted: have
Deleted: been
Deleted: are
Deleted: all
Deleted: very
Deleted: and
Deleted: (so that they show distinct black-white contrast)
Deleted: are
Deleted: In this irradiation condition it
Deleted: ¶
Deleted: very
Deleted: 40
Deleted: are
Deleted: very
Deleted: Many
Deleted: also
Deleted: appears

fields. We quote from Wen *et al* [15]: *"Mutual elastic interactions between clusters was found to affect their distribution and motion drastically. Because of mutual interaction, two clusters that are oriented along non-parallel crystallographic directions will either coalesce forming a larger one or rotate and pin one another at a short distance and move jointly in the same direction. Once two clusters are pinned together, they have less chance to change their orientation, and therefore their motion becomes almost pure one-dimensional. As this process proceeds, some additional clusters may be trapped into this pinned structure by changing their Burgers vectors."*

Wen *et al*'s model appears to be a good description of our experimental observations. Several of its distinctive features are seen experimentally. These include:(1) the formation of strings by the interaction of mobile ½<111> loops; (2) the observation that small clusters of 2-3 loops are still mobile, performing 1-D motion although with reduced mobility, but that larger clusters are immobile; and (3) the formation of groups of loops with the same Burgers vectors. The tendency of loops to form strings along <110> directions is likely to be due to loop-loop elastic interactions, where loops adjust their orientations and positions in order to minimize the elastic interaction energy [16].

What is the nature of the loops which participate in this process? Loops of both vacancy and interstitial nature with ½<111> Burgers vectors are thought to be mobile, according to simulations by Gilbert *et al* [17]. However the large loops which develop from strings have been shown to be of interstitial nature. We therefore believe that the strings consist of small interstitial loops. Initially it would be expected that small interstitial clusters would move in 1-D. Such 1-D motion would result in little recombination with V clusters. In thin foils both surfaces act as sinks and most interstitial clusters will be lost. We envisage that in thicker regions of foil, some clusters penetrate to the foil interior, where they can grow and interact, leading to the formation of immobile strings.

The development of large interstitial loops

Video evidence suggests that loop strings evolve into resolvable loops. Loops form at the sites of loop clusters or strings, and both the resolvable loops and the loop strings have ½ <111> Burgers vectors. Wen *et al* [15] find that groups of 5 or more loops are immobile and it seems reasonable to suppose that these strings act as the nuclei for large interstitial loops. The loops in the string would be expected to climb and coalesce by a similar mechanism seen for the larger loops as they develop into finger loops, as described below.

The changes in the shapes of loops as they grow – flexing – seems most likely to be due to glide of loops on their glide cylinders under the influence of stresses induced by the electron and ion beams. Note that the loops have large shear components - the finger-loops A analyzed in §3 lie close to the (111) plane but have Burgers vector $\mathbf{b} = \frac{1}{2}[\bar{1}11]$, so that the angle between the loop normal **n** and **b** is about 70°. This implies that loop growth involves both glide and climb. Overall the tendency is for loops to grow larger in all dimensions, implying a net absorption of interstitials. Occasionally loops seemed to shrink, possibly when a vacancy cluster was absorbed, although again glide may be involved.

Loops may climb by absorbing either single point defects and sub-microscopic clusters or resolvable loops. In videos we see loop growth and shrinkage without any obvious involvement of smaller loops, and we take this as evidence of the first process. However, small mobile loops still form continuously during irradiation and can be assimilated by larger loops This process seems to involve

Deleted: described above
Deleted: We have seen directly that
Deleted: appears to involve
Deleted: s
Deleted: between ½
Deleted: mobile
Deleted: .
Deleted: Small
Deleted: still
Deleted: . Larger
Deleted: (5 or more loops) become
Deleted: . Wen *et al*'s process leads to groups
Deleted: Most of these features are seen in our experiments.
Deleted: We note h
Deleted: that the next stage in microstructural evolution is the development
Deleted: in the same regions
Deleted: from strings
Deleted: of large
Deleted: interstitial
Deleted: loops which
Deleted: ¶
¶
Why do loop strings form only in thicker regions of foil? This must be due to the surfaces acting as strong sinks for small mobile interstitial loops or crowdion clusters.
Deleted: loops
Deleted: Some loops would move to the surface and be lost
Deleted: I
Deleted: will
Deleted: their interaction leads
Formatted: Indent: First line: 0"
Deleted: ¶
Deleted: analysed
Formatted: Font: Bold
Deleted: is

first the decoration of a larger loop by smaller loops, as seen in Figure 5. In the videos bright dots often appeared at the peripheries of large loops, then faded, suggesting absorption onto the dislocation line causing climb. Again this is consistent with the simulations of Wen *et al* [15]. In their study of dislocation decoration they find that small clusters are often trapped near the cores of line dislocations, where they can reorient their Burgers vectors to become parallel to that of the line dislocation and finally be absorbed.

The development of finger loops

Finger loops are formed by the coalescence of overlapping large interstitial loops. Details of the coalescence mechanism remain unclear. It probably involves both climb and glide.

Attempts to model loop coalescence by R. Novokshanov (private communication) by dislocation dynamic simulations are in an early stage. The modeling done so far is only for edge loops. This has shown that when hexagonal edge loops overlap in the z (foil normal) direction they can coalesce by the glide of segments on their joint slip plane. This leads to a stepped habit plane. This may be relevant in understanding how large finger loops can form without intersecting the foil surface - they may not lie entirely on a single habit plane, but would be stepped. The smaller constituent loops may initially have large edge components, but the average habit plane is close to the foil plane. Further simulations better reflecting the geometry of our experiments are in progress.

Other aspects of the development of finger loops also remain unclear. It would seem that initially all variants of ½ <111> loops are present. Why should only one set of loops in a local area develop into elongated loops? The tendency for such loops to align parallel to each other and close to <110> directions is presumably a consequence of their elastic interaction. But why should the favoured variant be such that the resulting elongated loops tend to lie along the foil thickness gradient (ie pointing towards the hole in the foil)? This may be a consequence of local stresses produced by bending, but at present we have no detailed answer to this question.

The effect of irradiation temperature and Cr content

Damage development at RT in UHP Fe seemed to follow the same pattern as at 300°C except that complex damage structures developed at somewhat higher doses. Damage development in the Fe8%Cr alloy seemed to show the same qualitative pattern as in UHP Fe. This suggests that damage processes remain essentially unchanged. At low doses in 300°C irradiations, loop sizes in Fe8%Cr and UHP Fe were very similar, although loop number densities were lower in Fe8%Cr (see Table 2). At higher doses, loop strings formed on a finer scale and this led to a finer distribution of resolvable large loops, smaller maximum loop sizes and a larger loop number density. This might be a consequence of a lower mobility of small loops in Fe8%Cr compared with pure Fe.

5. Conclusions

1. We have studied damage development under 150 keV Fe^+ ion irradiation in UHP Fe and an Fe8%Cr alloy. Initially isolated small dislocation loops formed, as described in Part 1.

2. At doses greater than about $2x10^{18}$ ions m^{-2} (~1 dpa) more complex microstructures developed in thicker regions of the foils, seeming to involve cooperative alignment and interaction of smaller loops. The exact mechanism by which this occurred is still unclear.

Deleted: 6
Deleted: 4
Deleted: ¶
Deleted: It is clear from our experiments that large f
Deleted: develop
Deleted: neighboring
Deleted: smaller
Deleted: when they overlap
Deleted: ¶
Deleted: pure
Deleted: pure
Formatted: Superscript
Deleted: The main effect of Cr seems to be a somewhat
Deleted: finer distribution of
Deleted: , and consequently a
Deleted: .
Deleted:
Deleted: ¶
Deleted: s

3. In UHP Fe irradiated at 300°C the damage developed into resolvable interstitial loops with ½<111> Burgers vectors. By a dose of $2x10^{19}$ ions m^{-2} (13 dpa), large (several hundred nm) finger-shaped loops had developed in some areas by the growth and subsequent coalescence of smaller loops. These loops had large shear components.

4. Similar strings of loops developed in UHP Fe irradiated at RT, but these had not developed further by the end of the experiment at 1.6×10^{19} ions m^{-2} (~ 10 dpa).

5. Damage development was similar in Fe8%Cr, although the finger-shaped loops seen in the 300°C irradiation were less developed and not as well aligned as in UHP Fe.

6. A plausible sequence of events leading to the observed damage structures has been described. It has been suggested that the presence of small glissile clusters is important in determining the evolution of damage structures.

Acknowledgements

The IVEM-Tandem Facility (within the Electron Microscopy Center at ANL) is supported by the US DOE Office of Science and operated under contract no. DE-AC02-06CH11357 by UChicago Argonne, LLC. We thank Dr. A. Liu and P Baldo of Argonne National Lab for their help in using this facility. . Part of this work was funded by the UKAEA, Culham Science Centre. *Ex-situ* experiments on UHP Fe were supported by the European Commission in the framework of the PERFECT Project. We also thank Prof. J. Le Coze of the École de Mines de Saint Étienne for the provision of UHP iron and Prof S. G. Roberts and Dr. S. L. Dudarev for helpful discussions

References

1. Z. Yao, M. Hernandez-Mayoral, M. L. Jenkins and M. A. Kirk, Phil. Mag. this issue (2008)
2. M L Jenkins and M A Kirk, Characterisation of Radiation Damage by Transmission Electron Microscopy, Institute of Physics Series in Microscopy in Materials Science (Series Editors, B Cantor and M J Goringe) ISBN 0 7503 0748 X (hbk) (2001)
3. I.M. Robertson, M.A. Kirk, Wayne E. King, Scripta Met. 18 317 (1984)
4. M.A. Kirk, I.M. Robertson, M.L. Jenkins, C.A. English, T.J. Black, and J.S. Vetrano. J. Nucl. Mater.**149** 21 (1987)
5. S. J. Zinkle, B.N. Singh. J. Nucl. Mater. **351** 269 (2006).
6. A F Calder and D J Bacon, J. Nucl. Mater. 207 25 (2000)
7. Yu. N. Osetsky, D. J. Bacon, B. N. Singh, B. Wirth, J. Nucl. Mater. **307-311** 852 (2002)
8. A F. Calder, D. J. Bacon, A. V. Barashev and Yu. N. Osetsky, Phil. Mag. Lett. **88**, 43(2008)
9. B von Guerard, D Grasse and J Peisl, Phys. Rev. Lett, **44** 262 (1980)
10. M.L Jenkins, C.A English and B L Eyre, Phil. Mag., **38** (1978).
11. H. Abe, N. Sekimura and T. Tadokoro, Mat. Trans. 46, 433 (2005)
12. J.L.Brimhall and B. Mastel, Rad. Effects **3**, 201 (1970)
13. M. Edrup, B. L. Singh, S.J . Zinkle et al J. Nucl. Mater. **307-311** 912 (2002)
14. B.N. Singh, J. H. Evans, A, Horsewell et al J. Nucl. Mater. **258** 865 (1998)
15. M. Wen, N.M.Ghoniem and B.N.Singh, Phil. Mag. 85, 2561 (2005)
16. R.S.Barnes, J.Phys. Soc. Japan. Suppl III **18** 305 (1963)
17. M Gilbert , S. L. Dudarev, P. Derlet, and D. G. Pettifor submitted to Phil. Mag (2007)

Tables

g \b	½ [111]	½ [$\bar{1}$11]	½ [1$\bar{1}$1]	½ [11$\bar{1}$]	[100]	[010]	[001]
1$\bar{1}$0	0	1	1	0	1	1	0
$\bar{1}$01	0	1	0	1	1	0	1
01$\bar{1}$	0	0	1	1	0	1	1
002	1	1	1	1	0	0	2
1$\bar{1}$0	0	1	1	0	1	1	0
0$\bar{1}$1	0	0	1	1	0	1	1
$\bar{1}$12	1	2	0	1	1	1	2
$\bar{1}$21	1	2	1	0	1	2	1
10$\bar{1}$	0	1	0	1	1	0	1
2$\bar{1}$1	1	1	2	0	2	1	1
1$\bar{1}$2	1	0	2	1	1	1	2

Table 1: |**g.b**| table for reflections near [111], [110], [311] and [131] poles.

Doses (ions m^{-2})	Average size (nm) (total number of measured loops)		Maximum size (nm)		loop density ($x10^{14}$ m^{-2})	
	UHP Fe	**Fe8Cr**	**UHP Fe**	**Fe8Cr**	**UHP Fe**	**Fe8Cr**
1 x 10^{18} (0.6 dpa)	2.95 ± 0.07 (1544)	3.4 ± 0.03 (391)	9	8	5.16 ± 1.72	2.22±0.5
2 x 10^{18} (1.3 dpa)	5.34 ± 0.09 (2358)		32		6.85 ± 2.05	
5 x 10^{18} (3.2 dpa)		4.9 ± 0.3 (402)		16		3.58±1
1 x 10^{19} (6.5 dpa)	9.7 ± 0.2 (2205)	5.2 ± 0.5 (1381)	92	20	7.05 ± 2.32	7.40±2.14
2 x 10^{19} (13 dpa)	10.4 ± 0.3 4.46±0.05 (2459)	5.5 ± 0.2 (1589)	224	24	2 .46 ± 0.7	9.68±2.61

Table 2: Quantitative data on sizes and densities of dislocation loops in UHP-Fe and Fe8%Cr irradiated at 300°C

Deleted: ¶
Doses (ions m^{-2}) ... [2]
Formatted: Font color: Auto
Formatted Table
Formatted: Font color: Auto
Formatted: Font color: Auto
Formatted: Font color: Auto
Formatted: Font color: Auto
Formatted: Font color: Auto
Formatted: Font color: Auto
Formatted: Font color: Auto
Formatted: Font color: Auto
Formatted: Font color: Auto
Formatted: Font color: Auto
Formatted: Superscript

Figure captions

Figure 1: Damage development in UHP Fe irradiated with 150 keV Fe^+ ions at 300°C seen in an *ex-situ* experiment. BFK images taken with $\mathbf{g} = 1\bar{1}0$ at doses (a) 2 x 10^{18} ions m^{-2} (~1.3 dpa); (b) 10^{19} ions m^{-2} (~6.5 dpa); (c) 2 x 10^{19} ions m^{-2} (~13 dpa). Images (a) and (c) were obtained with the foil oriented near (111) and image (b) was taken near the [001] pole.

Figure 2: Size distributions of loops in UHP Fe irradiated with 150 keV Fe^+ ions at 300ºC seen in an *ex-situ* experiment.

Figure 3: Development of damage structures in UHP Fe irradiated with 150 keV Fe^+ ions at 300°C. Note the change of scale in the bottom micrographs. Weak-beam micrographs taken with $\mathbf{g} = 1\bar{1}0$. Doses are (a) 10^{18} ions m^{-2} (0.6 dpa) (b) 2 x 10^{18} ions m^{-2} (1.2 dpa); (c) 10^{19} ions m^{-2} (6.5 dpa) (d) 1.6 x 10^{19} ions m^{-2} (10.4 dpa).

Figure 4 The formation of resolvable loops from loop strings in UHP Fe irradiated with 150 keV Fe^+ ions at 300°C. This is a series of frames extracted from video 3 at doses between 0.85 x 10^{19} ions m^{-2} (~5.6dpa) and 10^{19} ions m^{-2} (6.5 dpa). The white dotted line is drawn to the left of the feature of interest as a guide to the eye. Weak-beam images in $\mathbf{g} = 1\bar{1}0$ shown as negatives.

Figure 5. A series of frames grabbed from a video recording, showing loop growth and coalescence in UHP Fe irradiated with 150 keV Fe^+ ions at 300°C over a dose range from about 10^{19} ions m^{-2} (~6.5 dpa) to about 1.6 x 10^{19} ions m^{-2} (~10 dpa). Weak-beam micrographs taken with $\mathbf{g} = 1\bar{1}0$. The projection of the Burgers vector of the loops is shown.

Figure 6 Contrast experiment in UHP Fe irradiated with 150 keV Fe^+ ions to a dose of 1.6 x 10^{19} ions cm^{-2} (~ 10 dpa) at 300°C. The large loops have ½ <111> Burgers vectors. The Thompson tetrahedron indicates the (111) foil orientation for the $\{1\bar{1}0\}$ micrographs (a)-(d). The 002 micrograph (e) was taken close to the [110] pole. See the text for details.

Figure 7 Stereogram for the contrast experiment shown in Figure 8. The approximate position of the foil normal is marked FN. Loop set A has Burgers vector $\mathbf{b} = \pm ½[\bar{1}11]$, set B has $\mathbf{b} = \pm ½[1\bar{1}1]$] and set C has $\mathbf{b} = \pm ½[11\bar{1}]$.

Figure 8 Possible voids in UHP Fe irradiated at 300°C to a dose of 10^{19} m^{-2} (about 6.5 dpa). The features ringed appear as black dots in the overfocussed image on the left, and white dots in the underfocussed image, consistent with the contrast expected of small voids.

Figure 9 Development of an inhomogeneous damage structure in thicker areas of foil in UHP Fe irradiated with 150 keV Fe^+ ions at to a dose of 10^{19} m^{-2} (about 6.5 dpa) at RT. Strings of loops are seen in thicker areas, lining up more or less parallel to projection of the [110] direction. The inset shows the strings at higher magnification. Contrast

Deleted: near [111] pole
Deleted: [
Deleted:]
Deleted: [
Deleted:]
Deleted: Figure 2: . Damage development in UHP Fe irradiated with 150 keV Fe^+ ions at 300ºC (a) in foil of thickness > 100 nm: (b) in a thinner wedge-shaped region of foil. In both cases $\mathbf{g} = 1\bar{1}0$.¶
Deleted: 3
Deleted: 4
Deleted: $1\bar{1}0$.
Formatted: Font color: Auto
Formatted: Font color: Auto
Formatted: Font color: Auto
Formatted: Font color: Auto
Formatted: Font color: Auto
Formatted: Font color: Auto
Formatted: Font color: Auto
Formatted: Font color: Auto
Formatted: Font color: Auto
Formatted: Font color: Red
Deleted: 5
Formatted: Justified
Deleted: 6
Deleted:
Deleted: ¶ ¶ Figure 7
Deleted: Alignment of loops, seen when the foil (which is fairly close ... [3]
Deleted: 8
Deleted: Orientations of elongat ... [4]
Deleted: [
Deleted:]
Deleted: 10
Deleted: ¶ ... [5]
Formatted ... [6]
Deleted: Loops in UHP Fe irrad ... [7]
Deleted: ¶
Formatted ... [8]
Deleted: 12
Deleted: 13

experiments showed that the loops in a given string all have the same ½ <111> Burgers vector. In thin areas of foil, to the bottom right, only isolated loops are seen. Most of these have <100> Burgers vectors.

Figure 10 Evolution of microstructure with dose in Fe8%Cr irradiated with 150 keV Fe^+ ions at 300°C to doses of : (a) 10^{19} m^{-2} (~6.5 dpa) ;(b) 2 x 10^{19} m^{-2} (~13dpa). Micrograph (a) was taken under weak-beam conditions, and micrograph (b) under kinematical bright-field conditions.

Figure 11 Evolution of microstructure with dose in Fe8%Cr irradiated at RT with 150 keV Fe^+ ions to doses of (a) 10^{19} m^{-2} (~6.5 dp); and (b) 1.9 x 10^{19} ions m^{-2} (~12 dpa). Micrograph (a) was taken under weak-beam conditions, and (b) under kinematical bright-field conditions.

Deleted: (see Figure 14)

Deleted: ¶
Figure 14

Deleted: Contrast experiment showing the loops in a string all have the same ½ <111> Burgers vector. Foil orientation [001]. Both sets of loops are seen in **g** = 002: just one set is visible in each of the **g** = $\{\bar{1}10\}$ reflections. Strings line up more or less parallel to the [110] and $[\bar{1}10]$. These are displaced aperture images, so the resolution is relatively poor. The ferromagnetism of the specimen prevented the formation of on-axis weak-beam images of higher resolution.¶

Deleted: 15

Deleted: (a) 10^{18} m^{-2} (~0.65 dpa);

Deleted: b

Deleted: c

Deleted: s

Deleted: and (b) were

Deleted: c

Deleted: 16

Deleted: (a) 3 x10^{18} m^{-2} (~2 dpa); (b) 6 x10^{18} m^{-2} (~3.9 dpa);

Deleted: c

Deleted: d

Deleted: s

Deleted: - (c) were

Deleted: d

Page 5: [1] Deleted Mike Jenkins 6/20/2008 11:41:00 AM

Figure 7 shows loop alignment more clearly. Here the same specimen seen in Figure 6 has been tilted to [001], and a nearby area showing more organized loop alignment has been imaged under BFK conditions. Lines of loops can be seen along or close to the $[1\bar{1}0]$ direction running diagonally from the top left, and some have coalesced to form finger-shaped loops, similar to those seen in figure 1(b). These loops belong to the set designated A in the Burgers vector analysis described below. The $[1\bar{1}0]$ direction along which they align lies close to the plane of the foil. The tendency for alignment shown in this micrograph may be exaggerated because the foil has been tilted such that the loop habit plane, which is close to the plane of the foil, is inclined, see below. There is some evidence for more limited alignment in the perpendicular [110], direction which is steeply inclined to the foil plane, suggesting the formation of a raft-like structure.

Although there

Page 15: [2] Deleted Mike Jenkins 7/11/2008 9:16:00 AM

Doses (ions m^{-2})	Average size (nm) (total number of measured loops)	Maximum size (nm)	loop density ($x10^{14}$ m^{-2})
1 x 10^{18} (0.6 dpa)	2.95 ± 0.07 (1544)	9	5.16 ± 1.725.16
2 x 10^{18} (1.3 dpa)	5.34 ± 0.09 (2358)	32	6.85 ± 2.056.85
1 x 10^{19} (6.5 dpa)	9.7 ± 0.2 (2205)	92	7.05 ± 2.327.05
2 x 10^{19} (13 dpa)	10.4 ± 0.3 4.46±0.05 (2459)	224224	2 .46 ± 0.72 .46

Page 16: [3] Deleted Mike Jenkins 6/20/2008 12:31:00 PM

Alignment of loops, seen when the foil (which is fairly close to [111] in orientation) is tilted close to the [001] pole, and imaged in under bright-field kinematical conditions with $\mathbf{g} = 200$. UHP-Fe irradiated at 300˚C with 150keV Fe^{+} to $1.6x10^{19}$ ions m^{-2}(~ 10 dpa).

Page 16: [4] Deleted Mike Jenkins 6/20/2008 12:32:00 PM

Orientations of elongated loops at various positions relative to the hole in the TEM specimen. The foil thickness in the wedge-shaped specimen increases radially.

Figure 9

Page 16: [5] Deleted Mike Jenkins 6/20/2008 12:32:00 PM

Figure 11

Page 16: [6] Formatted Mike Jenkins 6/20/2008 12:32:00 PM

Indent: Left: 0", First line: 0"

Page 16: [7] Deleted **Mike Jenkins** **6/20/2008 12:32:00 PM**

Loops in UHP Fe irradiated with 150 keV Fe^{+} ions to 1.6 x 10^{19} ions m^{-2} (~ 10 dpa). BFK micrographs taken with $\mathbf{g} = 1\bar{1}0$. Micrographs (a) and (b) show a stereo pair, taken near the [111] and [110] poles respectively. Micrograph (c) is the same as (a) but has been shrunk perpendicular to **g** to simulate the foreshortening caused by tilting.

Page 16: [8] Formatted **Mike Jenkins** **6/20/2008 12:38:00 PM**

Indent: Left: 0", Hanging: 1"

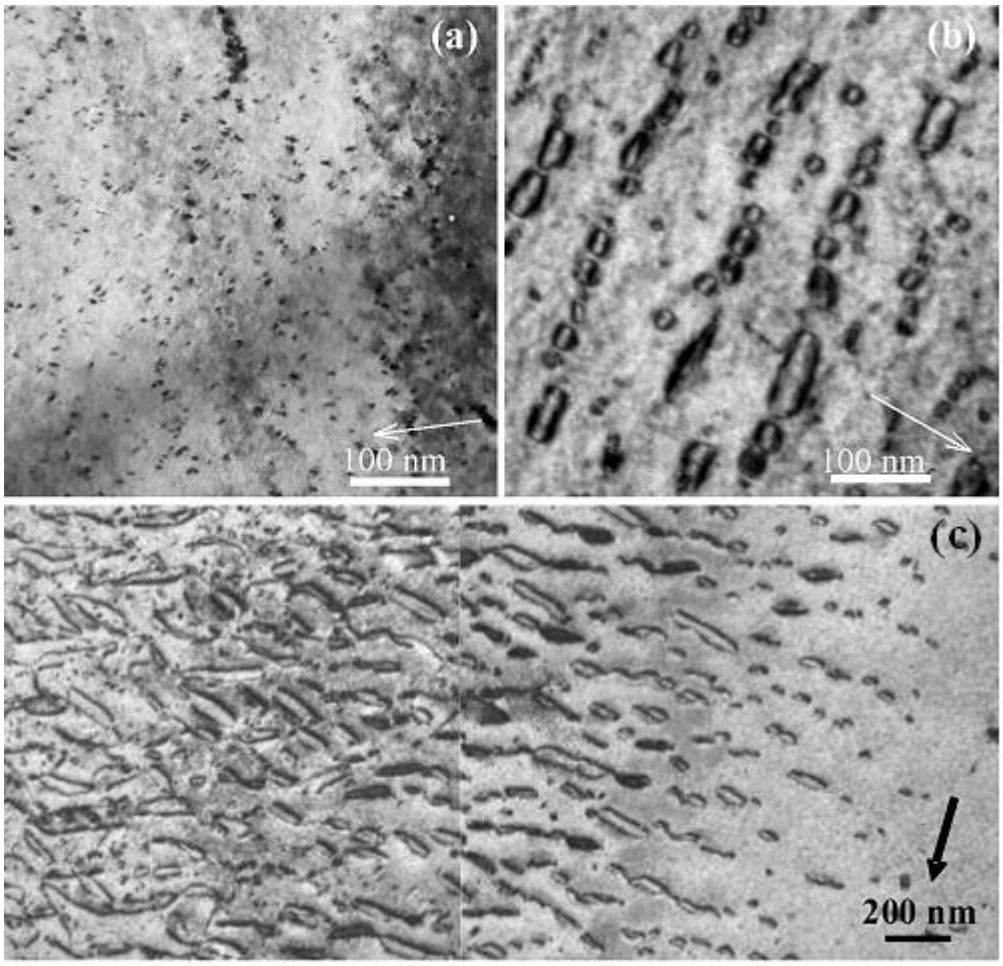

Figure 1
42x40mm (300 x 300 DPI)

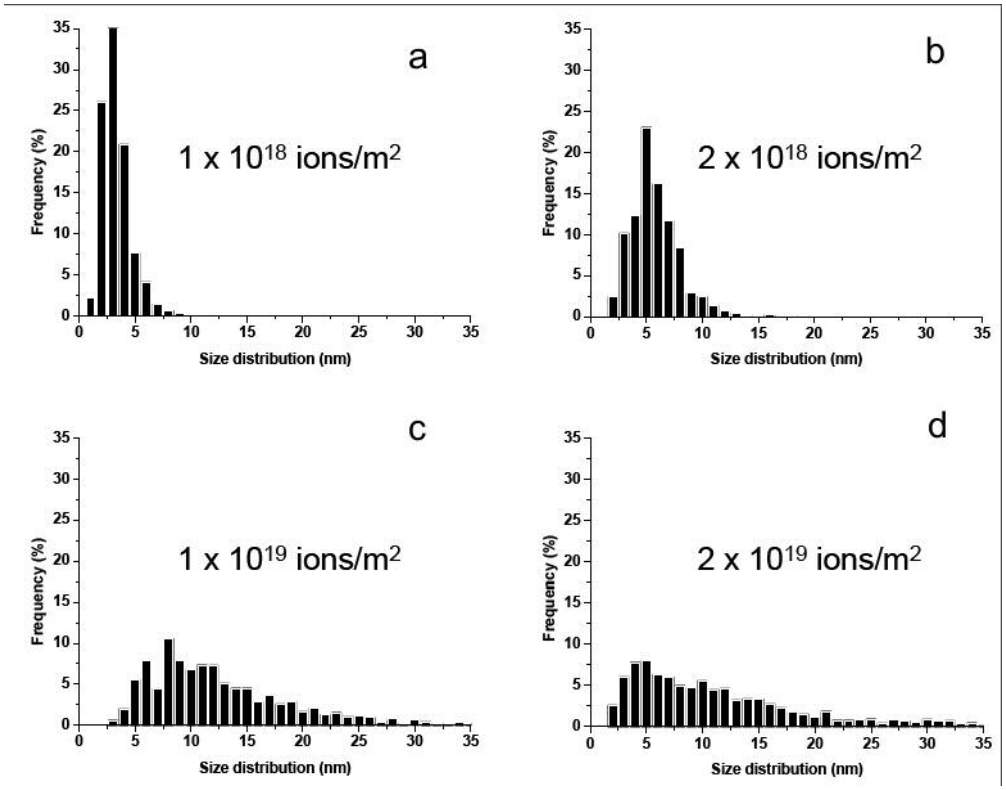

Figure 2

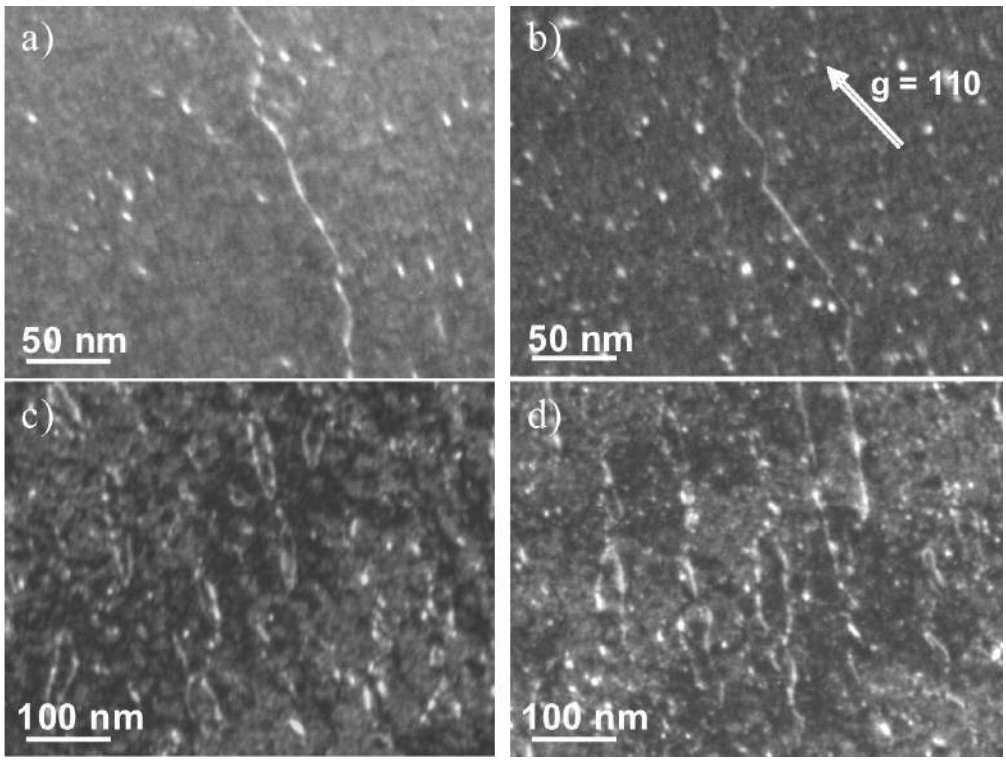

Figure 3

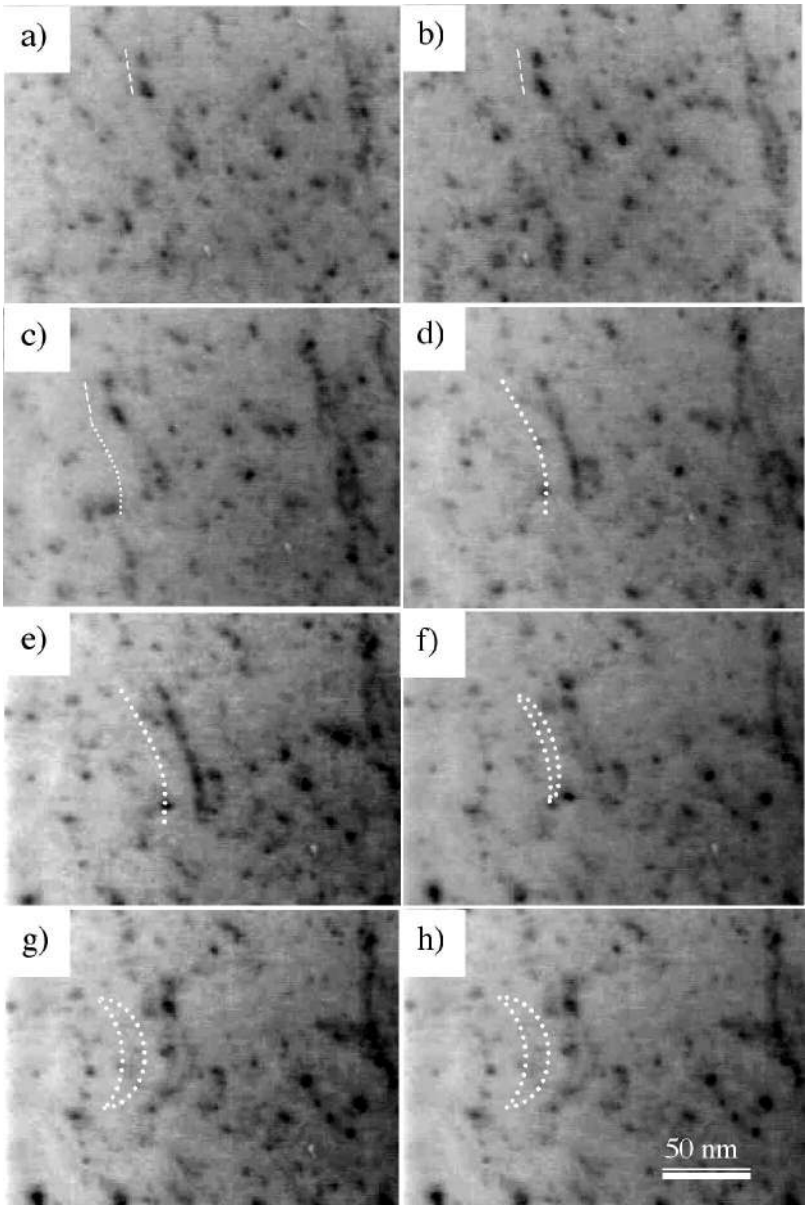

Figure 4
115x172mm (300 x 300 DPI)

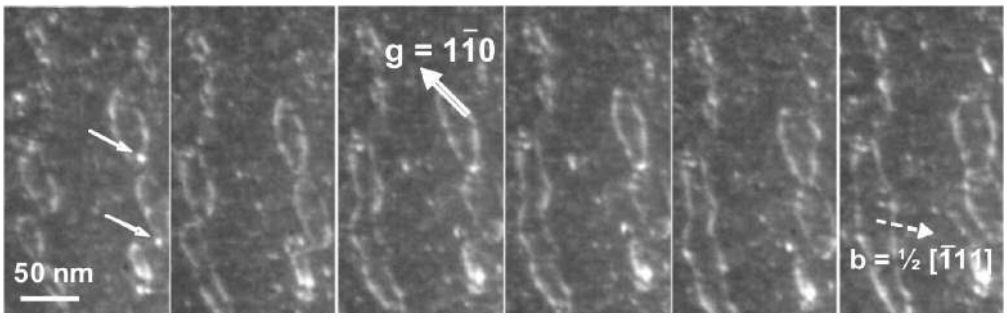

Figure 5

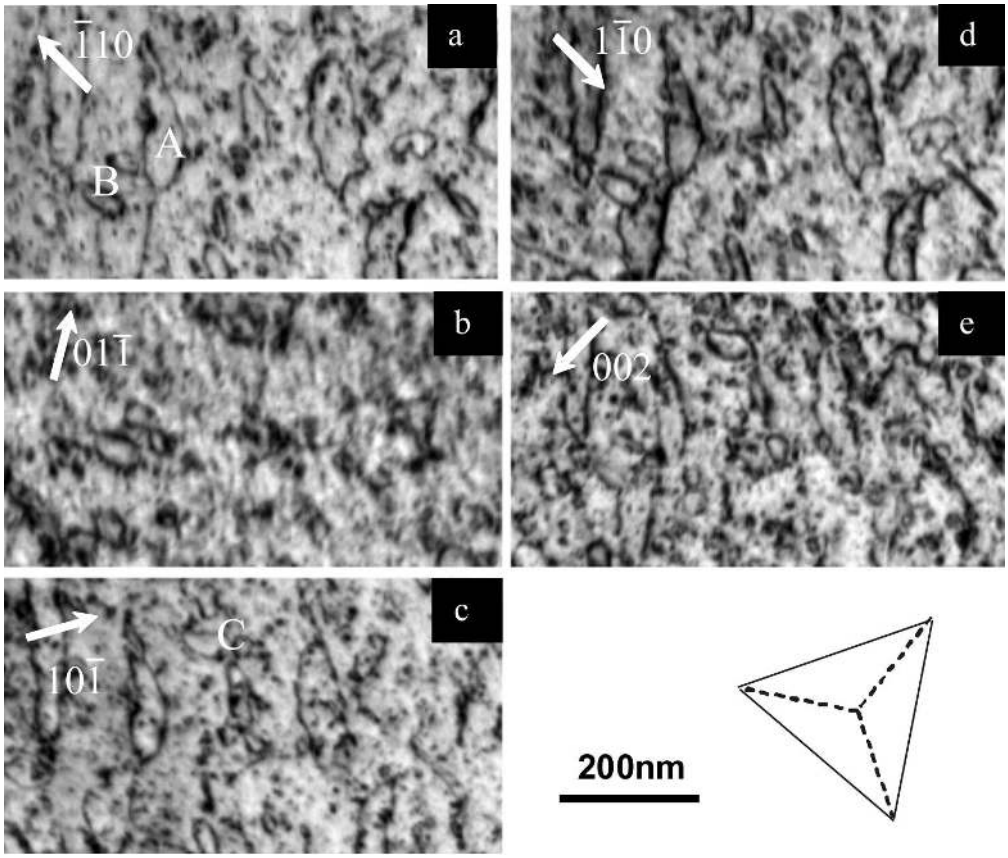

Figure 6

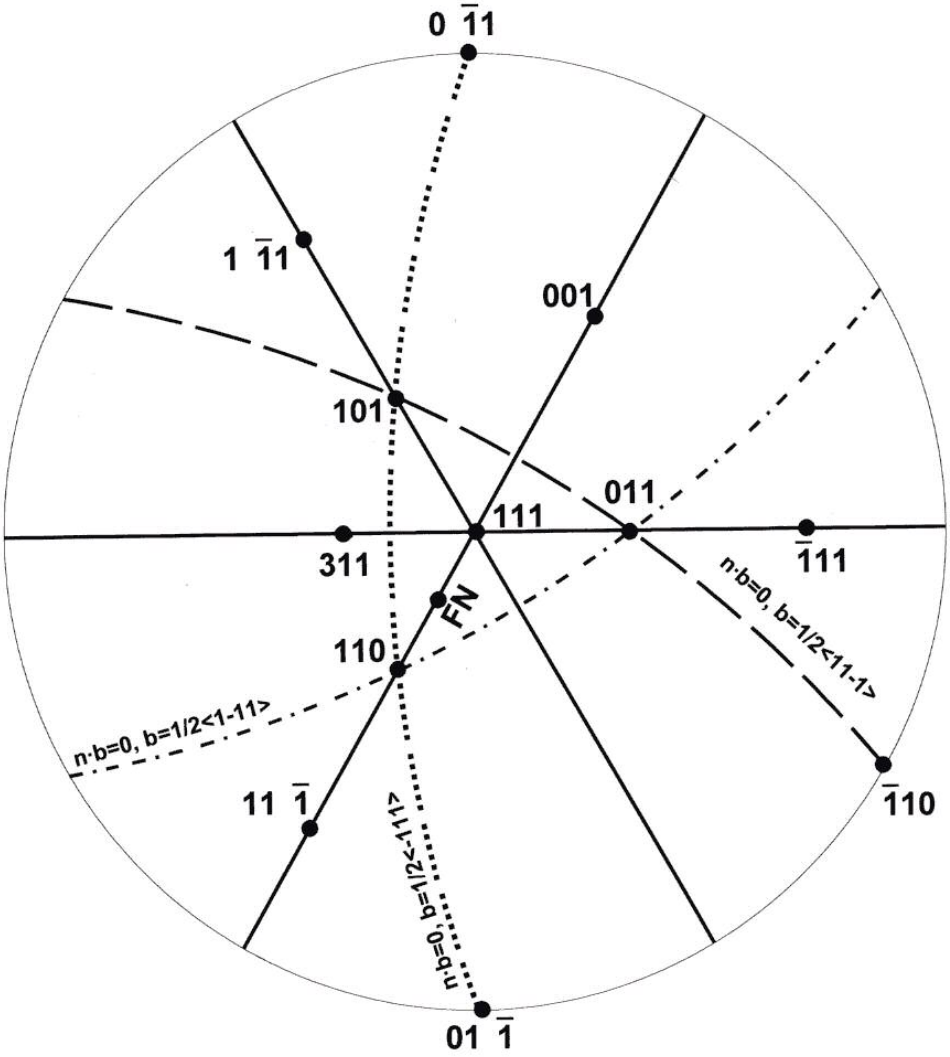

Figure 7
153x169mm (150 x 150 DPI)

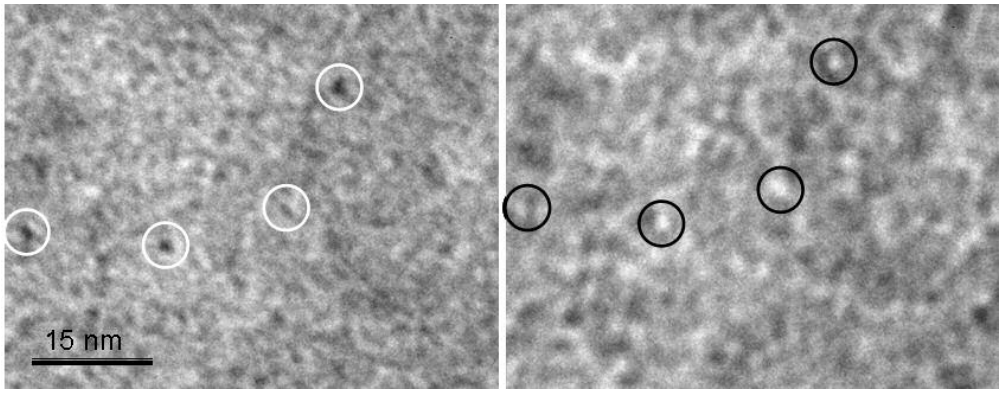

Figure 8
297x114mm (72 x 72 DPI)

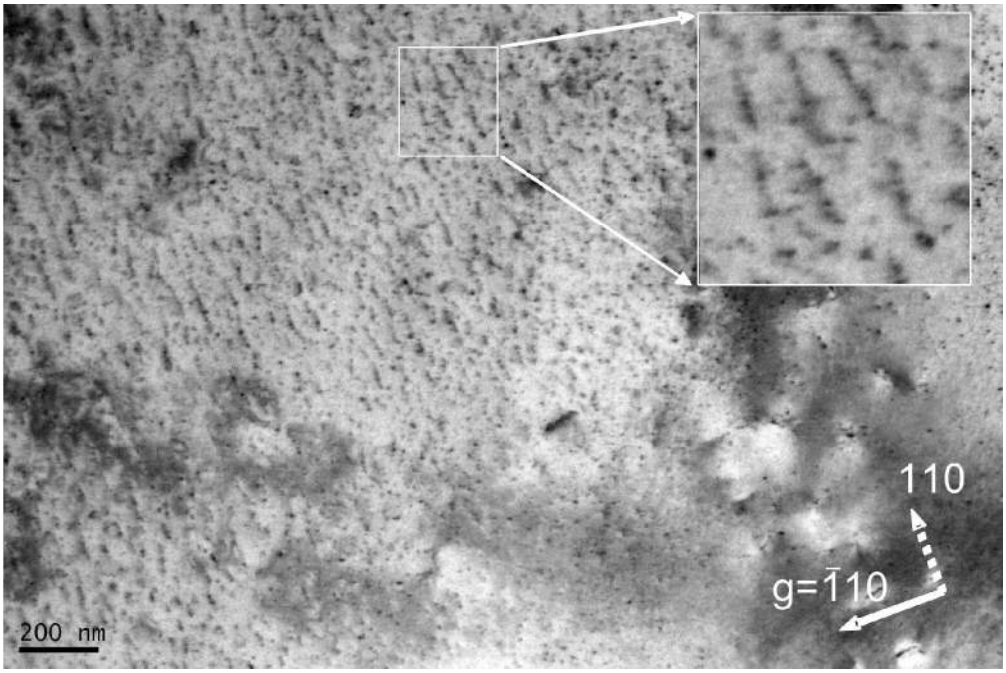

Figure 9

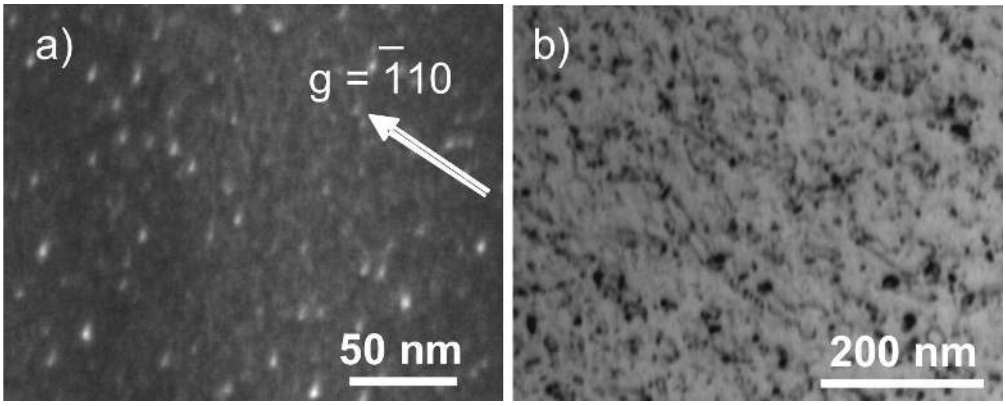

Figure 10

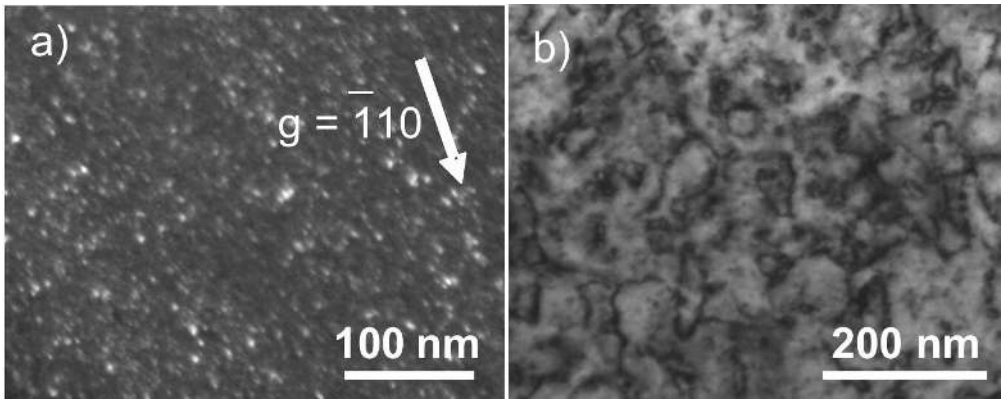

Figure 11